AGU PUBLICATIONS

Radio Science

RESEARCH ARTICLE
10.1002/2015RS005933

Key Points:
- GNSS positioning performance was evaluated under severe ionospheric condition
- TEC map developed in this study for scintillation mitigation improved the positioning performance
- Two interpolation method or the proper use of TEC map was conducted and compared

Correspondence to:
J. Park,
jihye.park@oregonstate.edu

Citation:
Park, J., V. Sreeja, M. Aquino, C. Cesaroni, L. Spogli, A. Dodson, and G. De Franceschi (2016), Performance of ionospheric maps in support of long baseline GNSS kinematic positioning at low latitudes, *Radio Sci.*, *51*, doi:10.1002/2015RS005933.

Received 7 JAN 2016
Accepted 20 APR 2016
Accepted article online 22 APR 2016

Performance of ionospheric maps in support of long baseline GNSS kinematic positioning at low latitudes

J. Park[1], V. Sreeja[2], M. Aquino[2], C. Cesaroni[3], L. Spogli[3,4], A. Dodson[2], and G. De Franceschi[3]

[1]School of Civil and Construction Engineering, Oregon State University, Corvallis, OR, USA, [2]Nottingham Geospatial Institute, University of Nottingham, Nottingham, UK, [3]Istituto Nazionale di Geofisica e Vulcanologia (INGV), Rome, Italy, [4]Space Earth Technology, Rome, Italy

Abstract Ionospheric scintillation occurs mainly at high and low latitude regions of the Earth and may impose serious degradation on GNSS (Global Navigation Satellite System) functionality. The Brazilian territory sits on one of the most affected areas of the globe, where the ionosphere behaves very unpredictably, with strong scintillation frequently occurring in the local postsunset hours. The correlation between scintillation occurrence and sharp variations in the ionospheric total electron content (TEC) in Brazil is demonstrated in Spogli et al. (2013). The compounded effect of these associated ionospheric disturbances on long baseline GNSS kinematic positioning is studied in this paper, in particular when ionospheric maps are used to aid the positioning solution. The experiments have been conducted using data from GNSS reference stations in Brazil. The use of a regional TEC map generated under the CALIBRA (Countering GNSS high-Accuracy applications Limitations due to Ionospheric disturbances in BRAzil) project, referred to as CALIBRA TEC map (CTM), was compared to the use of the Global Ionosphere Map (GIM), provided by the International GNSS Service (IGS). Results show that the use of the CTM greatly improves the kinematic positioning solution as compared with that using the GIM, especially under disturbed ionospheric conditions. Additionally, different hypotheses were tested regarding the precision of the TEC values obtained from ionospheric maps, and its effect on the long baseline kinematic solution evaluated. Finally, this study compares two interpolation methods for ionospheric maps, namely, the Inverse Distance Weight and the Natural Neighbor.

1. Introduction

Global Navigation Satellite Systems (GNSS) have been used in support of various applications such as precision agriculture, offshore operations, geodesy, surveying, mapping, land management, construction, and so on. With the evolution of the GNSS techniques, including new generation GNSS, improvements in receiver hardware/software, and processing algorithms, high-accuracy GNSS positioning is possible nearly anywhere in the world. However, problems still remain over certain regions, for example, in Brazil, whose territory sits around the area of the equatorial ionization anomaly (EIA) centered approximately 15° in latitude on either side of the geomagnetic equator, which are frequently affected by harsh ionospheric conditions [*Sreeja et al.*, 2012]. High-accuracy GNSS positioning is challenging in Brazil not only due to the frequent occurrence of scintillation (characterized by rapid fluctuations in the amplitude and phase of transionospheric radio signals) and the rapid variations of total electron content (TEC) but also due to the density of the available permanent GNSS networks, where the distance between stations can reach up to hundreds of kilometers, as, for example, in the São Paulo State based Real-Time Kinematic (RTK) network run by UNESP (São Paulo State University), the so-called URTKN (UNESP RTK Network). Despite these problems, GNSS is a highly demanding technique in Brazil where high-accuracy positioning is required in support of various applications such as precision agriculture, offshore, surveying, land management, civil aviation, and geodesy [*Park et al.*, 2015].

CALIBRA (Countering GNSS high-Accuracy applications Limitations due to Ionospheric disturbances in BRAzil), a project cofunded by the GNSS Supervisory Authority (GSA) under the European Commission Seventh Framework Program (FP7), aimed to develop carrier phase-based high-accuracy algorithms for RTK and Network RTK (NRTK) that are able to counter the adverse effects of ionospheric scintillation and sharp TEC gradients in Brazil.

The study described in this paper is part of the CALIBRA project outcomes and focuses on the long baseline GNSS kinematic solution with the aid of external information about the ionospheric delay. For a long baseline kinematic solution, the ionospheric delay is not easily canceled out by the double difference (DD) observable,

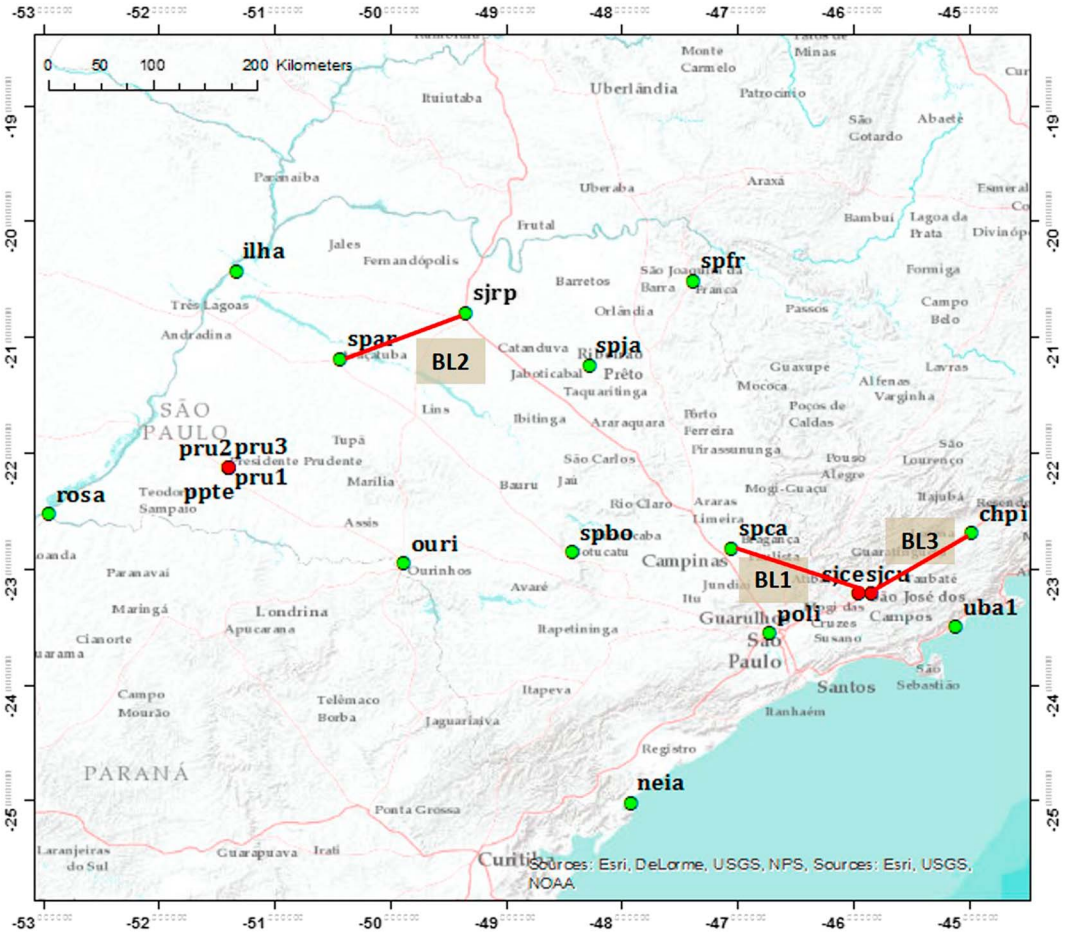

Figure 1. Google Earth image showing GNSS stations in São Paulo state including URTKN stations in green circles and CIGALA-CALIBRA network stations in red circles; selected baselines (BL1, BL2, and BL3) are indicated in red lines.

so that the residual DD ionospheric delay must be estimated separately [*Grejner-Brzezinska et al.*, 2004]. This method mostly relies on the suitable use of external ionospheric information, which is commonly provided via a so-called ionospheric map or TEC map. In this study, we developed a regional TEC map using a local GNSS network and compared its performance with that of the global ionospheric map. Experiments presented in this paper have been carried out using data from two GNSS networks in Brazil, namely, the URTKN, made up of 11 stations established in the state of São Paulo, and the Ionospheric Scintillation Monitoring Receiver network made up of 10 stations covering the Brazilian territory, referred to as CIGALA (CIGALA Concept for Ionospheric Scintillation Mitigation for Professional GNSS in Latin America)-CALIBRA network.

1.1. Ionospheric Scintillation

The global morphology of ionospheric scintillation occurrence is well known [*Basu et al.*, 2002], with peaks over the auroral to polar latitudes (65°N–90°N geomagnetic latitudes) and over the equatorial to low latitudes (20°N–20°S geomagnetic latitude). The processes governing the generation of scintillation are different over these two regions, leading to significant differences in the characteristics of the monitored scintillation effects [*Sreeja et al.*, 2011]. Scintillation at high latitudes is associated with large scale plasma structures and is generally controlled by the solar transients. However, at low latitudes, scintillation is not much dependent on the geomagnetic conditions and intense scintillation events can occur during the post sunset hours on geomagnetically quiet days. The most intense scintillation over these latitudes is associated with the crests of the EIA [*Aarons et al.*, 1980; *Basu et al.*, 1988]. Scintillation can impair the GNSS receiver signal tracking performance thereby leading to a degradation in the positioning accuracy [*Aquino et al.*, 2005; *Krankowski and Shagimuratov*, 2006; *Aquino et al.*, 2009; *Akala et al.*, 2012; *Sreeja et al.*, 2012].

The effect of the ionospheric delay on GNSS positioning is highly related to the ionospheric conditions at the two stations constituting the baseline, with the unmodeled DD ionospheric residuals propagating into the positioning error. *Alfonsi et al.* [2011] made the first attempt to correlate the variability of the electron density gradients and scintillation activity using data from high latitudes. The climatological assessment of the rate of TEC (ROT) on irregularities scales of few to tens of kilometers, and its related distribution by means of ROT standard deviation mapping was presented. A deeper investigation about the correlation between the occurrence of amplitude scintillation (as measured by the amplitude scintillation index, S4) and the standard deviation of ROT over the Brazilian equatorial and low latitudes was discussed in *Spogli et al.* [2013], where it is clearly demonstrated that the occurrence of scintillation significantly correlates with regional fluctuations of TEC gradients. To better focus on the spatial gradients of TEC, a recent study by *Cesaroni et al.* [2015] shows the correspondence between S4 occurrence and the standard deviation of the N-S TEC gradients, thus indicating the variable N-S TEC gradients as the principal driver of amplitude scintillation.

This paper describes experiments involving long baseline GNSS kinematic positioning under different scintillation conditions. The experiments have been conducted using different TEC maps and techniques, applied in the context of the kinematic data processing.

1.2. Data Description

In Figure 1, red placemarks indicate Septentrio PolaRxS receivers, designed for ionospheric TEC and scintillation monitoring deployed during the CIGALA-CALIBRA projects. The GNSS receivers constituting the URTKN are shown in yellow placemarks, consisting of geodetic receivers (JAVAD, Ashtech, Trimble, Leica, etc.). To perform the experiments as described in section 3, the largest sampling rate (15 s) provided by the URTKN has been used.

For the purpose of this work, positioning results are evaluated considering one of the receivers as a simulated rover. This allows the comparison between the kinematic positioning solution and the actual coordinates (known) of the simulated rover. Three baselines of about 100 km were chosen, namely, BL1: SPCA-SJCU (rover), 121.5 km; BL2: SPAR-SJRP (rover), 120.7 km; and BL3: CHPI-SJCU (rover), 115.3 km. Such baselines have been selected according to the data availability and with the aim to cover two different geographic regions in the São Paulo state. SJCU receiver is one of the CIGALA-CALIBRA network stations while SPCA, SPAR, SJRP, and CHPI are typical geodetic GNSS receivers: station SPCA is equipped with a LEICA GRX1200, stations SPAR and SJRP with TRIMBLE NETR8, and station CHPI with a JAVAD TRE_G3T.

2. Impact of TEC Map

2.1. Long Baseline RTK Mathematical Model

Equation (1) below represents the dual frequency double difference (DD) variables for GNSS observations:

$$\begin{cases} \Phi_{ij,1}^{kl} = \rho_{ij}^{kl} - I_{ij,1}^{kl} + T_{ij}^{kl} + \lambda_1 N_{ij,1}^{kl} 1 + m_{ij,1}^{kl} + \varepsilon_{ij,1}^{kl} \\ \Phi_{ij,2}^{kl} = \rho_{ij}^{kl} - I_{ij,2}^{kl} + T_{ij}^{kl} + \lambda_2 N_{ij,2}^{kl} + m_{ij,2}^{kl} + \varepsilon_{ij,2}^{kl} \\ C_{ij,1}^{kl} = \rho_{ij}^{kl} + I_{ij,1}^{kl} + T_{ij}^{kl} + M_{ij,1}^{kl} + e_{ij,1}^{kl} \\ P_{ij,2}^{kl} = \rho_{ij}^{kl} + I_{ij,2}^{kl} + T_{ij}^{kl} + M_{ij,2}^{kl} + e_{ij,2}^{kl} \end{cases} \quad (1)$$

where superscripts k and l and subscripts i and j represent satellites and stations, respectively, $\Phi_{ij,1}^{kl}$ and $\Phi_{ij,2}^{kl}$ are the DD carrier phase observables of L1 and L2, respectively, $C_{ij,1}^{kl}$ and $P_{ij,2}^{kl}$ are DD code pseudorange observables of L1 and L2, respectively, ρ_{ij}^{kl} is the DD range between the stations i and j and the satellites k and l, and $I_{ij,1}^{kl}$, $I_{ij,2}^{kl}$ are the DD ionospheric delays of L1 and L2, respectively. Note that these terms contain the first-order ionospheric delay only. T_{ij}^{kl} is the DD tropospheric delay; λ_1, λ_2 are the wavelengths of L1 and L2; $N_{ij,1}^{kl}$ and $N_{ij,2}^{kl}$ are the DD integer ambiguities on L1 and L2; $m_{ij,1}^{kl}$, $m_{ij,2}^{kl}$, $M_{ij,1}^{kl}$, and $M_{ij,2}^{kl}$ are multipath errors of the phase and code measurements on L1 and L2; and $\varepsilon_{ij,1}^{kl}$, $\varepsilon_{ij,2}^{kl}$, $e_{ij,1}^{kl}$, and $e_{ij,2}^{kl}$ represent the phase and code measurement noise on L1 and L2.

The tropospheric delay in equation (1) for this study is computed based on a total zenith delay (TZD) model and a mapping function (MF) for each ray path. The TZD was computed from Saastamoinen model [*Saastamoinen*, 1972] for both hydrostatic and wet delays with the standard atmosphere model as a meteorological data source. For the MF, the global mapping function (GMF) was applied [*Boehm et al.*, 2006]. This MF allows to calculate the TZD for each satellite-receiver link and, then, to remove its contribution in the GPS

observation. Integer ambiguity is searched by the Least Squares AMBiguity Decorrelation Adjustment algorithm [*Teunissen*, 1994] and the fixed/float solutions are determined using W-ratio test [*Wang et al.*, 1998]. It should be noted that this study only used GPS constellation.

The GNSS positioning solution can be obtained by applying the adjustment computation theory. Equation (2) shows the Gauss-Markov Model (GMM) for a DD GNSS solution with two stations, considering one station as a reference and another for which the coordinates need to be estimated.

$$y = A\xi + e, \quad e \sim \left(0, \sigma_0^2 W^{-1}\right) \tag{2}$$

The parameter determination for the GMM linear system is obtained by the least squares (LSQ) method. In equation (2), y is an observation vector, consisting of dual frequency GNSS observations, i.e., C, P, $\Phi 1$ and $\Phi 2$ as defined in equation (1), ξ is a parameter vector representing the corrections to be applied to the initial station coordinates as well as other unknown parameters like the delays due to the ionosphere, $I_{ij,1}^{kl}$, $I_{ij,2}^{kl}$ and the ambiguities affecting carrier phase measurement, A is a design matrix for the elements in ξ, and e is the observation error vector as a function of unit variance σ_0^2 and the weight matrix W.

For the kinematic solution, in the case of a short baseline and quiet ionospheric condition, it can be assumed that the ionospheric delays of the four ray paths in the DD observable cancel each other out and consequently that the ionospheric delay is negligible. However, for a long baseline and/or for disturbed ionospheric conditions, the DD ionospheric observable may contain a significant residual error, which must be estimated separately by introducing a constraint based on a priori (external) information about the ionosphere, as in equation (3):

$$\begin{cases} y = A\xi + e \\ z = K\xi + e_0 \end{cases}, \begin{bmatrix} e \\ e_0 \end{bmatrix} \sim \left(\begin{bmatrix} 0 \\ 0 \end{bmatrix}, \quad \sigma_0^2 \begin{bmatrix} W^{-1} & 0 \\ 0 & Q_0 \end{bmatrix} \right) \tag{3}$$

where z is the a priori information for the ionosphere, in this case, it can be used to predict the DD ionospheric delay terms of ξ, K is a design matrix, e_0 is the error vector of z, and Q_0 is the corresponding cofactor matrix.

If reliable TEC maps can be provided over the considered area, the DD ionospheric delay can be evaluated along each ray path which can be included in z, whose stochastic characteristic is defined by $\sigma_0^2 Q_0$.

2.2. Global Ionosphere Map (GIM) Versus CALIBRA TEC map (CTM)

There are several global and local ionospheric maps, which can be used as external ionospheric information in GNSS positioning. One of the most easily accessible products is the GIM provided by the IGS. The GIM product, used in the experiment described in section 3, consists of maps of vertical TEC (vTEC) obtained by averaging the maps coming from different data centers all around the world [*Hernández-Pajares et al.*, 2009], i.e., CODE (Center for Orbit Determination in Europe), ESA (European Space Agency), JPL (Jet Propulsion Laboratory), and UPC (Polytechnic University of Catalonia). The GIM are made available in IONEX (Ionosphere map Exchange) over a regular grid, with spatial and temporal resolution of $5° \times 2.5°$ (latitude/longitude) and 2 h, respectively.

In the CALIBRA project, the CTM, which fully covers the São Paulo state in Brazil, was generated by calibrating the slant TEC (sTEC) according to the method described below. Using both carrier phase and code delay observations, in the so-called geometry free combination, a new observable can be obtained as shown in equation (4):

$$\widetilde{L}_{\text{arc}} = \text{sTEC} + b_R + b_s + \langle \varepsilon_P \rangle_{\text{arc}} + \varepsilon_L \tag{4}$$

In equation (4), $\widetilde{L}_{\text{arc}}$ represents the carrier phase new observable "leveled" to the code delay one. The subscript arc refers to any continuous arc of observation, b_R is the bias associated to the receiver hardware, b_s is the bias of the satellite hardware, $\langle \varepsilon_P \rangle_{\text{arc}}$ refers to multipath and noise on the code delay observation averaged over an entire arc, and ε_L is the same errors on the carrier phase delay. sTEC is the slant TEC. ε_L can be neglected when compared with the errors that affect the code delay [*Braasch*, 1996].

In other calibration methods, $\langle \varepsilon_P \rangle_{\text{arc}}$ is also considered negligible [*Braasch*, 1996; *Mannucci et al.*, 1998] However, the experiment described in *Ciraolo et al.* [2007] involving two colocated receivers acquiring signal from the same antenna demonstrated that the contribution of $\langle \varepsilon_P \rangle_{\text{arc}}$ is not always negligible, thus suggesting to

maintain the $\langle \varepsilon_P \rangle_{\text{arc}}$ term in equation (4), thus estimating a unique bias for each arc instead of b_R and b_s separately for receivers and satellites, respectively. Thus, equation (4), representing the calibrated TEC, reduces to

$$\widetilde{L}_{\text{arc}} = \text{sTEC} + \beta_{\text{arc}} \tag{5}$$

In equation (5), β_{arc} is the arc offset, which is a constant to be estimated over each arc of observations related to a given receiver and satellite pair. β_{arc} represents the sum of $b_R$and b_s and the contribution of any nonzero averaged errors for, e.g., due to multipath. The sTEC is then projected to the vertical using a single layer approximation according to which the relationship between slant and vertical TEC is the following:

$$\text{vTEC} = \frac{\text{sTEC}}{F(\alpha_{\text{elev}})} \tag{6}$$

where

$$F(\alpha_{\text{elev}}) = \frac{1}{\sqrt{1 - \left(\frac{R_e \cos \alpha_{\text{elev}}}{R_e + H_{\text{IPP}}}\right)^2}} \tag{7}$$

Even if it is well known that the single layer model fails to describe the absolute values of electron density in case of global maps including the anomaly crests, in this study the simply approach used to retrieve sTEC and to project it on vertical is sufficient to feed the needs of the positioning technique for two main reasons: first, the region covered by this study is localized (latitude range: −23.21° to −22.12°; longitude range: −41.79° to −51.41°) and second, the network is dense enough to provide a good coverage of the region.

For the needs of the positioning technique used in this study, the crucial information is the TEC difference between the ionospheric pierce points (IPPs) relative to two different stations (master station and rover) for the same satellite. In other words, the error introduced by the mapping function is partially canceled out considering TEC gradients instead of absolute values of TEC [*Cesaroni et al.*, 2015].

Thus, maps of calibrated vertical TEC at IPPs over the São Paulo state region were created in both scattered data format, i.e., vTEC at each IPP, and grid format, i.e., vTEC in a regular grid, with 1° × 1° (latitude/longitude) of spatial resolution. The temporal resolution of both types of maps is 15 s. In this paper, the scattered vTEC map was used for experimental flexibility.

The GIM and the CTM were used to provide the a priori information in equation (3) for the long baseline GNSS kinematic processing and their performances were compared in terms of the positioning solution. It should be noted that the overall range of TEC values in both maps are in good agreement, except that the GIM is much smoother than the CTM.

In this study, the in-house GNSS positioning software developed under the CALIBRA project was used. This software is capable of adopting both grid type and scattered data point type of TEC maps for the stochastic constraints shown in equation (3). In order to minimize additional errors, precise orbit (IGS final product) was applied. The kinematic positioning process was conducted by doing least squares adjustment of epoch by epoch solution.

In addition, an investigation on the GIM precision has been carried out by applying different empirical biases for the TEC root-mean-square (RMS) provided in the GIM IONEX files. The aim of this investigation was to assess the impact of applying these biases when using the global TEC map under different ionospheric conditions. Finally, in order to assess the impact of different interpolation techniques when using a scattered TEC map, such as the CTM, a comparison of interpolation methods was carried out. Section 3 describes the experiments corresponding to the three above mentioned topics, which were performed under different scintillation conditions for long baseline kinematic processing and evaluated based on the positioning results.

3. Experiments

3.1. Performance of GIM and CTM on RTK

In this section, some case events for long baseline kinematic GNSS using the GIM and the CTM under quiet and disturbed ionospheric conditions are presented in terms of comparison between GIM and CTM performance. The ionospheric conditions are selected in accordance with the prevailing scintillation level identified with the PolaRxS receivers. As briefly mentioned in the introduction, there is a close relationship between

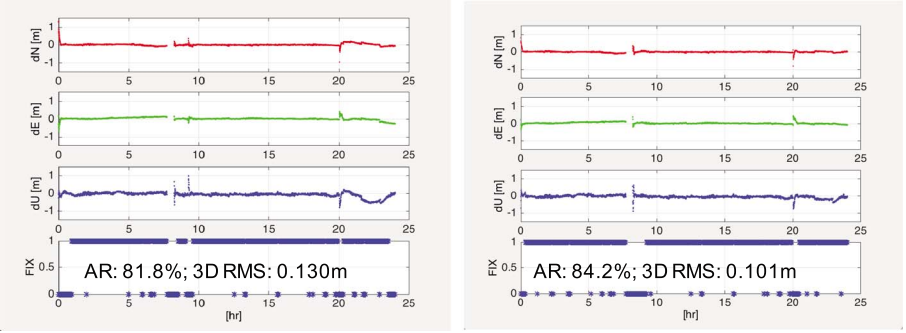

Figure 2. Kinematic positioning result of BL1 using the (left) GIM and using the (right) CTM on DOY141 2013 (time is in UT)—quiet day scintillation case; positioning error in north, east, and up components on the top three plots (dN, dE, and dU) and the ambiguity resolution index on the bottom plot (0—float, 1—fixed).

scintillation occurrence and TEC fluctuations and hence possibly presents more difficulties for RTK positioning where the incorrectly estimated DD ionospheric delay propagates to the positioning result. Therefore, throughout the experiments we used scintillation levels as a proxy for the state of the ionosphere and thus as an indicator of the TEC activity that may degrade RTK positioning performance. It should be noted that the scintillation level was determined based on the widely used amplitude scintillation index, S4 [*Van Dierendonck et al.,* 1993], which is monitored by the scintillation monitoring receivers in the CIGALA-CALIBRA network stations. In our study, the scintillation level is categorized into quiet, moderate, and strong where $S4 < 0.3$, $0.3 \leq S4 < 0.7$, and $S4 \geq 0.7$, respectively.

3.1.1. Quiet Scintillation Case

To evaluate GIM and CTM performance under quiet ionospheric conditions, positioning results over the SPCA-SJC1 baseline (BL1) (see Figure 1) were compared for DOY141 2013 (21 May 2013). The S4 index measured by the receiver in SJCU was below the moderate scintillation threshold (0.3) during most of the day. The kinematic positioning results using the GIM and the CTM are shown in the left and right panels, respectively of Figure 2. In each panel, dN, dE, and dU represents the positioning error in the north (dN, red), east (dE, green), and up (dU, blue). In addition, the ambiguity resolution (AR, bottom plots in blue) indices are shown (0—float, 1—fixed).

This experiment shows that during low scintillation conditions, both GIM and the CTM provide reliable ionospheric information leading to satisfactory and comparable positioning results. AR success rates are 81.8% with GIM and 84.2%, with CTM. The corresponding 3-D positioning RMSs are 0.130 m and 0.101 m and include both float and fixed solutions. The positioning performance using either of the maps is quite satisfactory if one considers the 15 s sampling rate and a 121.5 km baseline.

3.1.2. Strong Scintillation Case

Strong scintillation levels indicate the presence of steep spatial and temporal TEC gradients in the region. Such conditions are more challenging for the estimation of the a priori ionospheric information. In this section, some experiments under strong scintillation conditions are analyzed and the results of the kinematic positioning using GIM and CTM are compared. Figure 3 shows the time variations of the amplitude scintillation index S4 as measured at PRU1 (blue diamonds) and SJCU (green diamonds) on DOY269 2013. PRU1 and SJCU are located in the west and east regions of São Paulo state, respectively. From Figure 3, it can be observed that both receivers experienced moderate to strong levels of scintillation ($S4 > 0.3$) during night time and, in particular, during the local postsunset hours. For this day, kinematic positioning was conducted on BL2 and BL3 by making use of the GIM and the CTM. To detail the scintillation level, PRU1 receiver has been used to characterize BL2 and SJCU has been used to characterize BL3. Such selection has been made according to the proximity of the scintillation receivers in PRU1 and SJCU to the corresponding selected baselines. Similar to Figure 2, Figures 4 and 5 show the GNSS kinematic positioning results for BL2 (SPAR-SJRP, baseline length 120.7 km) and BL3 (CHPI-SJCU, baseline length 115.3 km) on DOY269 in 2013, respectively. Figures 4 (left) and 5 (left) refer to the use of GIM, while Figures 4 (right) and 5 (right) to CTM. For both baselines the AR success rates are considerably larger when using CTM (BL2: 36.6% – BL3: 67.1%) than GIM (BL2: 4.0% – BL3: 20.9%). Also, the 3-D positioning RMS is considerably lower when using CTM (BL2: 1.294 m – BL3: 0.403 m) than GIM (BL2: 2.279 m – BL3: 1.546 m). These results clearly indicate that the use of CTM improves

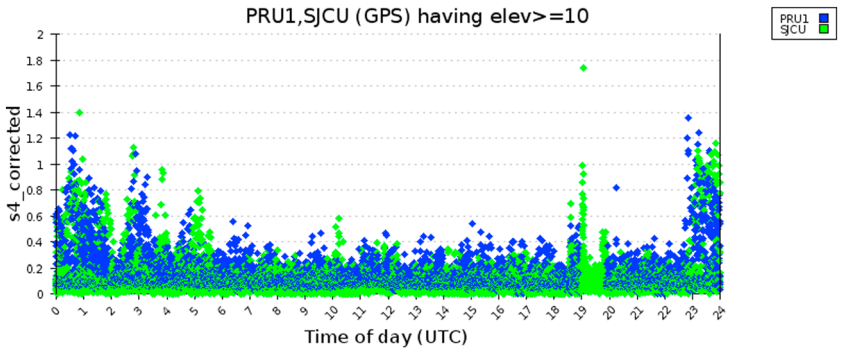

Figure 3. S4 recorded at PRU1 and SJCU on DOY269 2013 (time is in UT).

the AR meaningfully and reduces the 3-D positioning error with respect to the use of GIM. The AR success rate, when using either GIM or CTM, is still low under strong scintillation conditions, which can be attributed to the poor quality of the measurements. However, it can be seen from Figures 4 and 5 that even during these hours the use of the CTM led to more accurate float solutions.

To summarize the results of the experiments presented in the previous two sections and of other experiments not discussed here, Table 1 presents an overview of the comparison between GIM and CTM performance in providing the ionospheric a priori information. As mentioned before, this table also presents some experimental results referring to case events not explicitly discussed in this paper but have been presented here to give a more detailed picture of the GIM and CTM comparison tests. The other analyzed events presented in Table 1 clearly support the discussion stated for the case event here. To give a quantitative picture of the comparison between CTM and GIM, the last two columns of Table 1 report the percentage and the absolute (in meters) improvement in positioning accuracy of CTM against GIM.

The most intriguing feature is that the best performance of CTM with respect to GIM is obtained under moderate to strong scintillation level, both in terms of improved ambiguity resolution and of smaller 3-D error. However, it is noticeable that in two cases, the use of CTM leads to a negative improvement of the positioning performance. A possible explanation could be that even if the ambiguity integer is fixed, the obtained value is incorrect. However, the "worsening" (negative improvement) in the absolute 3-D positioning errors in these two cases is around 10 cm, which can be considered small compared to the improvement achieved under the strong scintillation cases, which range from 44 cm to 128 cm.

3.2. Impact of the Stochastic Property of the GIM on GNSS Positioning

The results in the previous section showed that the CTM worked significantly better than the GIM in most cases, especially under strong scintillation conditions. The possible reasons would be (1) the CTM represents the regional TEC with a better accuracy, (2) the spatial and temporal resolutions of the GIM are too low to

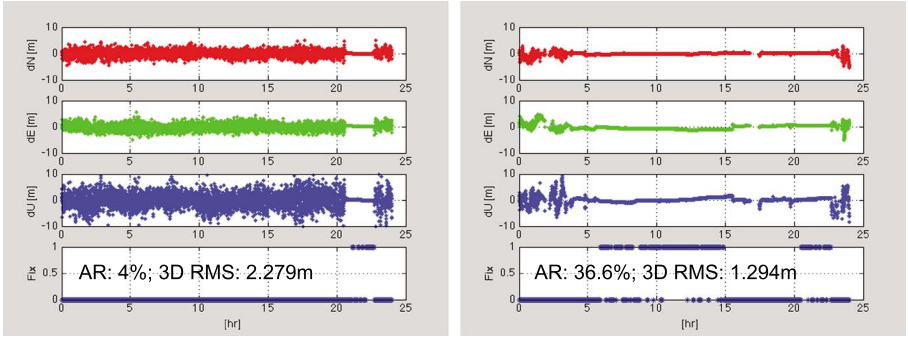

Figure 4. Kinematic positioning result of BL2 using the (left) GIM and using the (right) CTM on DOY269 2013 (time is in UT)—strong scintillation case; positioning error in north, east, and up components on the top three plots (dN, dE, and dU) and the ambiguity resolution index on the bottom plot (0—float, 1—fixed).

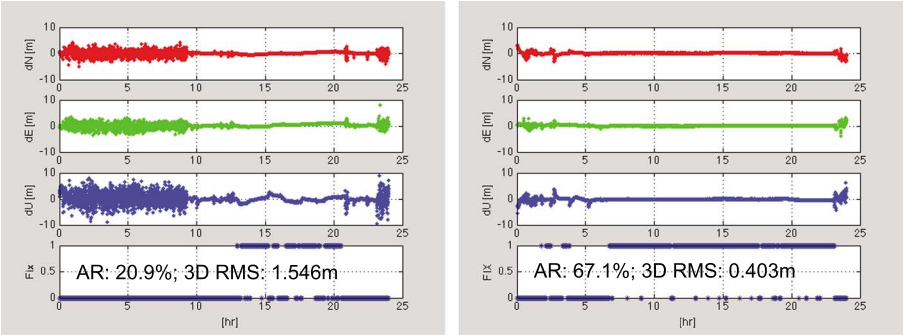

Figure 5. Kinematic positioning result of BL3 using the (left) GIM and using the (right) CTM on DOY269 2013 (time is in UT)—strong scintillation case; positioning error in north, east, and up components on the top three plots (dN, dE, and dU) and the ambiguity resolution index on the bottom plot (0—float, 1—fixed).

detect the local ionospheric disturbances, and (3) the hardware of the receivers forming the CIGALA/CALIBRA network, in particular their internal OCXO clock, is more accurate in the determination of the signal phase [*Bougard et al.*, 2011]. Since the GIM is provided every 2 h, it possibly smoothens out the high ROT effects, associated with strong scintillation occurrence. However, the GIM may represent an adequate option in regions where regional TEC maps are unavailable. This section introduces a method that was tested in the São Paulo state region, whereby the best possible solution for long baseline kinematic solutions can be achieved by using the GIM and which is possibly ready to be adopted in other areas.

The GIM contains vTEC values with a corresponding RMS in TEC units (TECU) in a regular grid provided in IONEX format. In order to apply the grid data provided in IONEX format to an arbitrary IPP, bivariate interpolation using the nearest 4 points of vTEC values can be used [*Schaer et al.*, 1998].

In equation (3), the mathematical model for long baseline RTK using the external ionospheric information was introduced so that the vTEC and vTEC RMS information from the GIM can be used in z and $\sigma_0^2 Q_0$, respectively. As mentioned earlier, the accuracy of vTEC is very important because it directly affects the stochastic model of the RTK positioning solution. It is also known that the vTEC and vTEC RMS in the GIM are computed based on four different vTEC maps generated independently at four centers (CODE, ESA, JPL, and UPC). However, it is not completely clear how the RMS values are derived and whether we should use these values indiscriminately because the vTEC RMS in the IONEX files is mostly near 1 TECU. In addition, the vTEC should be interpolated for a specific IPP location to be applied in the RTK solution, and this interpolation error must be determined and accounted for in the processing. Moreover, since neither the "true" vTEC RMS on each grid nor the interpolation error is predictable, an extensive trial-and-error investigation was carried out in order to estimate the optimal RMS values to be applied to the vTEC provided by the GIM.

Since the suggested interpolation for the GIM is the bivariate interpolation using only four grid points, the interpolation error in the distances would be the same. Therefore, we increase the RMS of the GIM by simply adding the different constant RMS values to the interpolated vTEC RMS from equation (3) in order to evaluate

Table 1. Summary of the Results Including More Cases

DOY, Year	Baseline	Scintillation Category	GIM		CTM		Improvement of 3-D RMS	
			AR (%)	3-D RMS (m)	AR (%)	3-D RMS (m)	(m)	(%)
141, 2013	BL1	Quiet	81.8	0.130	84.2	0.101	0.029	22.3%
141, 2013	BL2	Moderate	62.3	0.164	72.6	0.263	−0.099	−60.4%
269, 2013	BL2	Strong	4.0	2.579	36.6	1.294	1.285	49.8%
269, 2013	BL3	Strong	20.9	1.546	60.6	0.403	1.143	73.9%
21, 2014	BL3	Strong	17.3	1.193	58.6	0.749	0.444	37.2%
45, 2014	BL2	Strong	14.0	1.026	17.4	1.141	−0.115	−11.2%
AVG				1.106		0.659	40.4%	

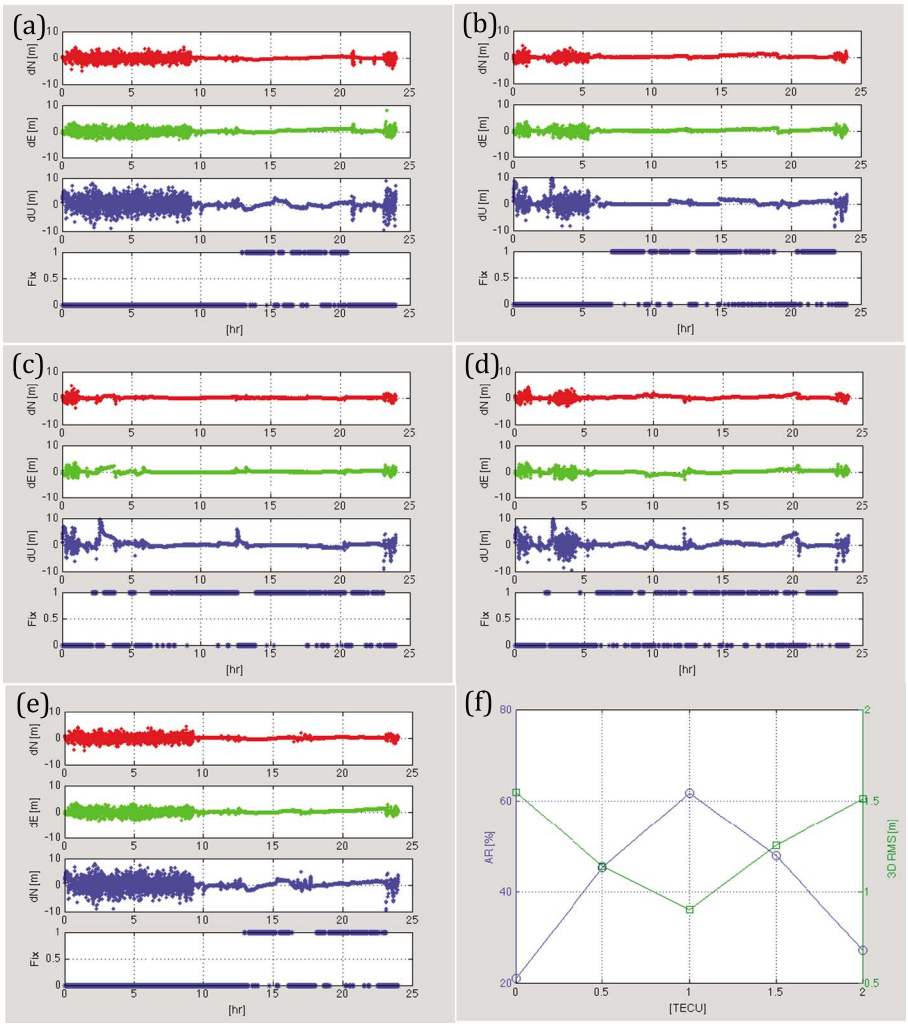

Figure 6. Kinematic positioning results by using the GIM with the additional vTEC RMS of (a) 0 TECU, (b) 0.5 TECU, (c) 1 TECU (top right), (d) 1.5 TECU, (e) 2 TECU for BL3, DOY269 in 2013, and (f) summary of positioning results using different vTEC RMS for GIM. In Figure 6f, the blue circles denote the AR success rate, while the green squares denote the 3-D RMS in meters.

the impact of additional uncertainty to the vTEC information and observed the corresponding kinematic positioning performance.

Figure 5 was introduced above to compare the kinematic results for BL3 on DOY269 in 2013 (strong scintillation day as shown in Figure 3) using the GIM and the CTM. The AR success rate was 20.9%, with 1.546 m for the 3-D positioning RMS when using the GIM. In this new experiment the RTK processing was carried out by increasing the constant vTEC RMS by additional values varying from 0 to 2 TECU in steps of 0.5 TECU. The positioning results are shown Figures 6a–6e. The 3-D positioning RMS and the AR success rate for each vTEC RMS value are depicted in Figure 6f and listed in Table 2.

Table 2. Kinematic Positioning Result of BL3 Using Different RMS for GIM; DOY269 in 2013

Additional RMS	AR Success Rate (%)	3-D Positioning Error (RMS) (m)
0 TECU (default)	20.9	1.546
0.5 TECU	45.1	1.139
1 TECU	61.7	0.903
1.5 TECU	47.8	1.253
2 TECU	27.1	1.511

Obviously, by introducing the different vTEC RMS values, significant changes are observed in terms of the positioning error (top three plots in each panel) and the AR success rate (bottom plot in each panel). By comparing the effect of the different vTEC RMS values, 1 TECU seems to be the optimal a priori uncertainty

Table 3. Kinematic Positioning Result of BL2 Using Different RMS for GIM; DOY45 in 2014

Additional RMS	AR Success Rate (%)	3-D Positioning Error (RMS) (m)
0 TECU (default)	14.0	1.026
0.5 TECU	13.6	1.117
1 TECU	19.9	1.090
1.5 TECU	13.7	1.196
2 TECU	6.0	1.593

to be introduced in the GIM, as it greatly improves the AR success rate and the positioning error. Another case study for a strong scintillation day, DOY45 in 2014, on BL2 was conducted and the positioning results are shown in Table 3.

In this case study, much lower changes were observed as compared to DOY269. However, it still indicates 1 TECU as the most effective vTEC RMS within this case study.

In addition, a case study on a moderate scintillation day was performed using BL2 on DOY141 2013, when S4 varied from 0.3 to 0.7. Again, the default vTEC RMS is computed by the bivariate interpolation from the RMS provided in IONEX. The experimental result for the RMS tests is shown in Table 4.

The kinematic positioning results using the default setting (0 TECU added) is relatively good when compared to the strong scintillation days in terms of AR success rate (62.3%) and 3-D positioning RMS (0.164 m), which must be due to the lesser impact of scintillation. Unlike the strong scintillation cases, the additional vTEC RMS did not greatly impact the positioning result. By adding 0.5 TECU, the AR success rate was slightly increased and the 3-D positioning RMS was comparable to the default setting (less than 1 cm difference).

From the case studies presented in this section, the optimal precision to be added to the GIM has been observed for each scenario. In order to compare these case studies, AR success rates and the 3-D positioning RMS are normalized and presented in Figure 7. The normalization was performed by dividing the values in each column of Tables 2, 3, and 4 (AR success rate and 3-D RMS, respectively) by the square root of the sum of the squared data values in the corresponding column.

It can be observed from Figure 7 that for the two strong scintillation days, highest AR success rate and lowest positioning error were observed when an uncertainty of 1 TECU was introduced in the stochastic model. Unlike the strong scintillation cases, for the moderate scintillation day, using 0.5 TECU in the stochastic model was enough to achieve the highest AR success rate and the positioning error was low for either 0 or 0.5 TECU. This result is reasonable in that the strong scintillation scenarios lead to bigger discrepancies when using the GIM. The overall conclusion from the analyses is that for a strong scintillation scenario, it is more important to allow a larger uncertainty to the GIM model than for a quiet/moderate scenario. From the limited experiments performed in this section it seems that an a priori vTEC RMS of 1 TECU could be used for the GIM to achieve a better performance during strong scintillation periods.

3.3. Interpolation Methods

vTEC from GNSS signals is essentially derived from sTEC values estimated along the signal ray paths between GNSS satellites and receivers on the ground. Therefore, the observations used as input to any GNSS based TEC map will be a scattered data set. For GNSS positioning (including RTK, NRTK, and PPP), the vTEC should be determined at a target location via a chosen interpolation method, and this procedure introduces an interpolation error. Since the objective of TEC maps is to provide users with accurate values, minimizing the interpolation error by using an appropriate method is crucial. In this study, we compared two interpolation methods, namely, the Inverse Distance Weight and the Natural Neighbor, using the CTM under different scintillation scenarios, and assessed the capability of each interpolation method in terms of the positioning performance over a long baseline kinematic positioning.

Table 4. Kinematic Positioning Result of BL2 Using Different RMS for GIM; DOY141 in 2013

Additional RMS	AR Success Rate (%)	3-D Positioning Error (RMS) (m)
0 TECU (default)	62.3	0.164
0.5 TECU	65.6	0.173
1 TECU	62.7	0.391
1.5 TECU	45.1	0.457
2 TECU	49.9	0.310

3.3.1. Inverse Distance Weight interpolation

Inverse Distance Weight (IDW) is one of the most commonly used techniques for scattered data points. The underlying assumption is that the interpolated value at a target location will be influenced mostly by the nearby points and less by the more

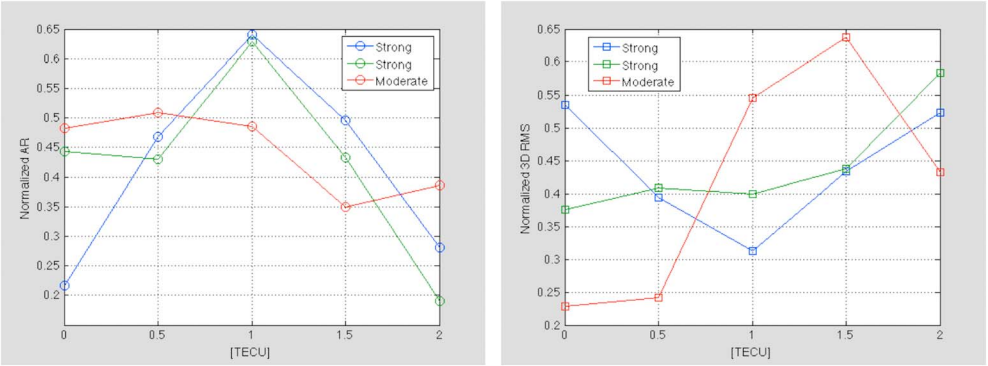

Figure 7. (left) Normalized AR success rates for different cases and (right) the corresponding normalized 3-D positioning RMS (right).

distant points. One of the simplest forms of the IDW is Shepard's method [*Lukaszyk,* 2004]. The typical IDW equation is represented in equation (4).

$$F(x,y) = \Sigma_{i=1}^{n} w_i f_i \tag{4}$$

where n is the number of scatter points in the data set, f_i are the scatter data sets, and w_i are the weight functions assigned to each scatter point. The weight function for Shepard's method is defined as $w_i = \frac{h_i^{-2}}{\Sigma_{j=1}^{n} h_j^{-2}}$ with $h_i = \sqrt{(x-x_i)^2 + (y-y_i)^2}$ for the 2-D coordinates (x, y) [*Shepard*, 1967].

3.3.2. Natural Neighbor Interpolation

The basic concept of the Natural Neighbor (NN) interpolation is identical to the IDW shown in equation (4), where the weight functions w_i are defined based upon Thiessen polygon network for the scatter data set. The weights used in NN interpolation are calculated based on the concept of local coordinates. In order to define the local coordinates for the interpolation point, P_n, the area of all Thiessen polygons in the network should be known. Figure 8 taken from http://www.xmswiki.com/xms/GMS:Natural_Neighbour shows an shows an example for the change in the Thiessen polygons when the interpolation point P_n is inserted. The dashed lines show the edges of the Thiessen network before P_n is inserted, and the solid lines show the edges of the Thiessen network after P_n is inserted.

The NN only uses the data values that are affected by inserting P_n in the network, so that the points 1, 4, 5, 6, and 9 are used for the interpolation in the above example figure. The weights, w_i, of those points are calculated by finding how much of each of the surrounding areas is influenced when inserting the target point into the Thiessen network,

$$w_i = \frac{k_i}{k}$$

where k is the Thiessen polygon area of P_n and k_i is the difference in the Thiessen polygon area of a neighboring scatter point, P_m, before and after P_n is inserted.

Although both methods basically originate from the same concept, which is the distance based weighting, the interpolated values using these two methods are sometimes significantly different. Figure 9 provides the interpolated vTEC of a ray path from one satellite, GPS PRN10, to one station, SJCU, (top) and the DD vTEC between two stations in BL3 on DOY293 in 2013 (bottom) for both interpolation algorithms. It can be observed from this figure that there is a significant difference between the two methods, and this will directly relate to the positioning result.

Figure 10 compares the kinematic positioning results using the two interpolation methods on DOY269 in 2013. The AR success rate and the positioning RMS using the IDW method are 63.3% and 0.752 m, while the results by applying the Natural Neighbor method are 60.6% and 0.515 m, respectively. It should be noted that the AR success rate using the Natural Neighbor method is lesser but the overall positioning RMS is better, which means some incorrectly fixed solutions from the IDW turned into float solutions with a lower positioning error. This can be seen from the plots of Figure 10, e.g., the big jump near 3–4 UT in dU in Figure 10 (left) has mostly disappeared in Figure 10 (right). This case also shows that the Natural Neighbor interpolation method would determine the TEC with a smaller interpolation error.

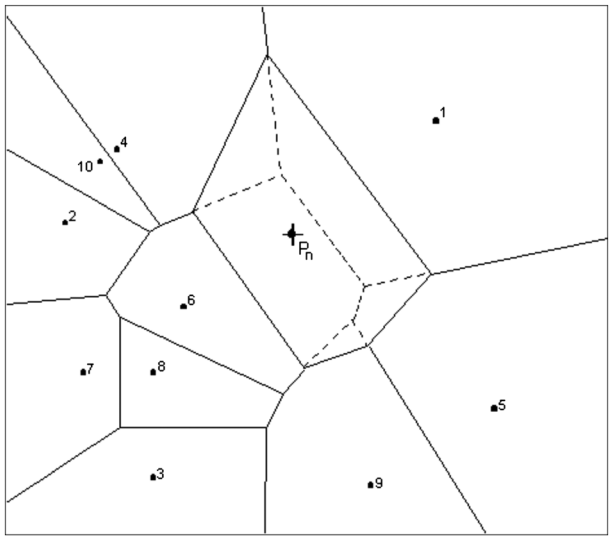

Figure 8. Overlapping Thiessen polygon areas used in computation of local coordinates (http://www.xmswiki.com/xms/GMS:Natural_Neighbor; accessed 3 December 2014).

Another strong scintillation case (BL2 on DOY45 in 2014) was also tested, and the kinematic positioning results are shown in Figure 11 for the IDW (left) and Natural Neighbor (right) interpolation methods.

The AR success rate and RMS using the IDW method are 10.2% and 1.322 m, while the results by applying the Natural Neighbor are 17.4% and 1.141 m, respectively. It should be noted that the positioning performance of this case study was much poorer than the previous case shown in Figure 10. This must be due to the correlation between the scintillation level and TEC spatial gradients which directly influences the kinematic positioning result. Although neither of the results in Figure 11 is satisfactory, the Natural Neighbor interpolation method still improves positioning performance. From the case studies presented in this section, it seems that while using the CTM in long baseline kinematic positioning, the Natural Neighbor interpolation method gives better results compared to the IDW under the different scintillation scenarios.

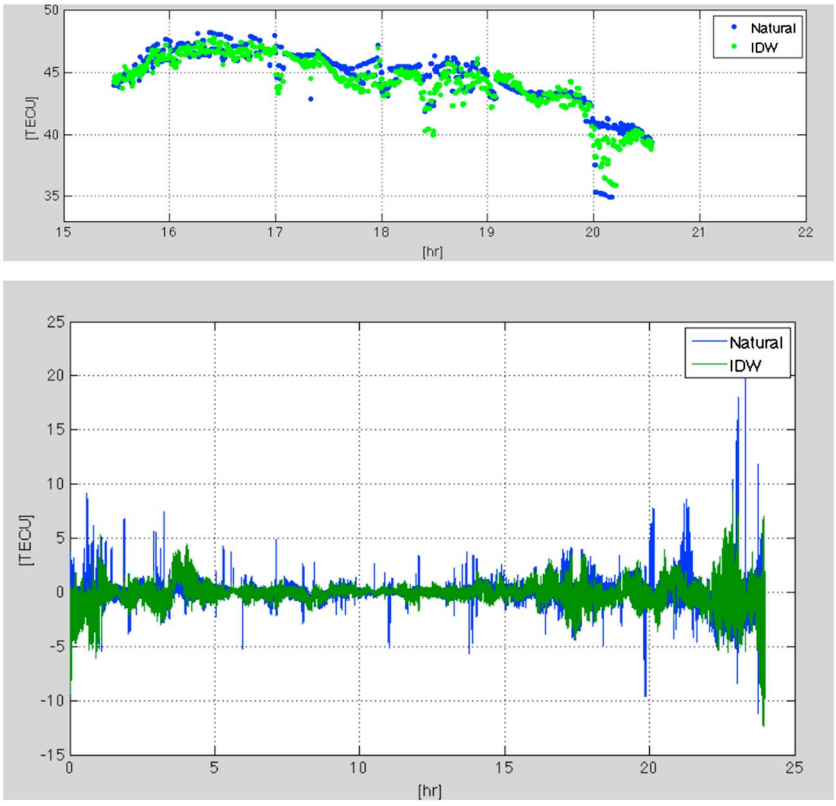

Figure 9. Interpolated TEC value of single satellite (PRN10) observed by (top) SJCU station and (bottom) DD TEC values of BL3 on DOY269 2013 in time series; green indicates IDW and blue indicates Natural Neighbor, time is in UT.

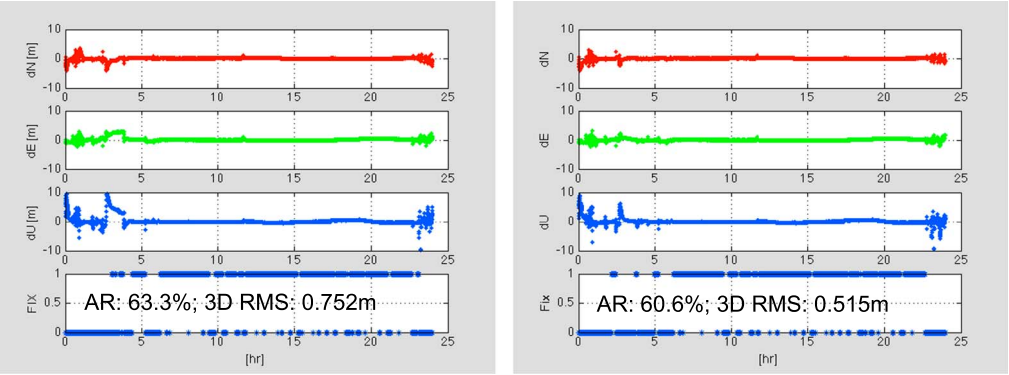

Figure 10. Interpolation comparison for a strong scintillation day (BL3, DOY269 in 2013, time is in UT); (left) IDW versus (right) Natural Neighbor.

4. Conclusion and Future Work

The effects of the ionosphere are crucial for high-accuracy GNSS positioning, in general, and become more significant in long baseline RTK positioning at low latitude regions, where scintillation and TEC fluctuations are frequently observed. In this study, we focused on the performance of different ionospheric maps in support of long baseline kinematic positioning in the Brazilian territory, which sits on an area of the Earth prone to ionospheric disturbances. In order to aid the ionospheric estimation in kinematic positioning, accurately modeled TEC information is essential. Within the CALIBRA project, the CTM was developed, which covers the region around São Paulo state, in Brazil. This paper assessed the performance of the CTM in comparison to the GIM with respect to their ability to improve positioning results.

From the presented case studies, it is clear that the CTM performs significantly better than the GIM under strong scintillation, as shown in Table 1. On average, our study showed that the CTM provides an improvement of 40.4% over the GIM in terms of positioning accuracy for the kinematic positioning performance. Furthermore, the uncertainty of the TEC values extracted from the external TEC map to be applied to the kinematic processing was investigated for the GIM. The experiments over the low latitudes show that at least 1 TECU must be added to the default TEC RMS in the GIM during periods of strong scintillation and 0.5 TECU under moderate scintillation periods. Finally, different interpolation methods for the CTM were also investigated in order to minimize the interpolation error for the scatter data set. From the experiments, the Natural Neighbor interpolation method performed better than the IDW interpolation.

In conclusion this study reveals that a highly accurate (regional) TEC map can improve kinematic positioning performance and that using an appropriate precision for the TEC map is also an important factor. Moreover, the interpolation method associated with the use of the map should be carefully chosen, as the interpolation error propagates and significantly affects the positioning performance. It should be noted that the suggested methods throughout this paper could be applied to not only the long baseline RTK but also NRTK and PPP.

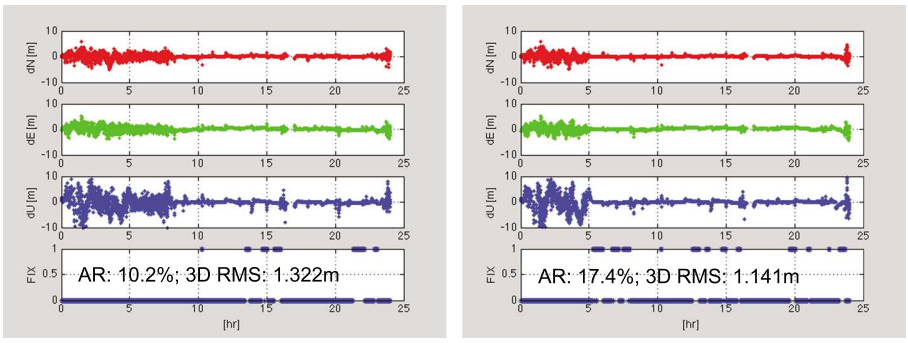

Figure 11. Interpolation comparison for strong scintillation day (BL2, DOY45 in 2014, time is in UT); (left) IDW versus (right) Natural Neighbor.

Acknowledgments
The CALIBRA project is funded under the EC Seventh Framework Program and is carried out in the context of the Galileo FP7 R&D program supervised by the GSA. The authors would like to thank all CALIBRA partners, UNESP (São Paulo State University, Brazil), Septentrio Satellite Navigation NV, INGV (Instituto Nazionale di Geofisica e Vulcanologia, Italy) and UNG (University of Nova Gorica, Slovenia) for their collaboration, and GSA for the financial support. The data related to this research work are stored in the CALIBRA data server (http://is-cigala-calibra.fct.unesp.br) and can be made available for free for research purposes.

References

Aarons, J., J. P. Mullen, H. E. Whitney, and E. M. Mackenzie (1980), The dynamics of equatorial irregularity patch formation, motion and decay, *J. Geophys. Res.*, *85*, 139–149, doi:10.1029/JA085iA01p00139.

Akala, A. O., Doherty, P. H., Carrano, C. S., Valladares, C. E., and Groves, K. M. (2012), Impacts of ionospheric scintillations on GPS receivers intended for equatorial aviation applications, *Radio Sci.*, *47*, RS4007, doi:10.1029/2012RS004995.

Alfonsi, L., L. Spogli, G. De Franceschi, V. Romano, M. Aquino, A. Dodson, and C. N. Mitchell (2011), Bipolar climatology of GPS ionospheric scintillation at solar minimum, *Radio Sci.*, *46*, RS0D05, doi:10.1029/2010RS004571

Aquino, M., T. Moore, A. Dodson, S. Waugh, J. Souter, and F. S. Rodrigues (2005), Implications of ionospheric scintillation for GNSS users in Northern Europe, *J. Navigat.*, *58*(2), 241–256.

Aquino, M., J. F. G. Monico, A. H. Dodson, H. Marques, G. De Franceschi, L. Alfonsi, V. Romano, and M. Andreotti (2009), Improving the GNSS positioning stochastic model in the presence of ionospheric scintillation, *J. Geod.*, *83*(10), 953–966, doi:10.1007/s00190-009-0313-6.

Basu, S., E. MacKenzie, and S. Basu (1988), Ionospheric constraints on VHF/UHF communication links during solar maximum and minimum periods, *Radio Sci.*, *23*, 363–378, doi:10.1029/RS023i003p00363.

Basu, S., K. M. Groves, Su. Basu, and P. J. Sultan (2002), Specification and forecasting of scintillations in communication/navigation links: Current status and future plans, *J. Atmos. Sol. Terr. Phys.*, *64*, 1745.

Boehm J., A. E. Niell, P. Tregoning, and H. Schuh (2006), Global Mapping Functions (GMF): A new empirical mapping function based on numerical weather model data, *Geophys. Res. Lett.*, *33*, L07304, doi:10.1029/2005GL025545.

Bougard B., J. M. Sleewaegen, L. Spogli, V. Sreeja, and J. F. G. Monico (2011), CIGALA: Challenging the solar maximum in Brazil with PolaRxS, *Proceedings of the 24th International Technical Meeting of the Satellite Division of the Institute of Navigation (ION GNSS 2011)*, Portland, OR, September 2011, pp. 2572–2579.

Braasch, M. S. (1996), Multipath effects, in *Global Positioning System: Theory and Applications*, chap. 14, vol. 1, pp. 547–568, American Institute of Aeronautics and Astronautics, Reston, Va, doi:10.2514/5.9781600866388.0547.0568.

Cesaroni C., et al. (2015), L-band scintillations and calibrated total electron content gradients over Brazil during the last solar maximum, *J. Space Weather Space Clim.*, *5*, A36, doi:10.1051/swsc/2015038.

Ciraolo, L., F. Azpilicueta, C. Brunini, A. Meza, and S. M. Radicella (2007), Calibration errors on experimental slant total electron content (TEC) determined with GPS, *J. Geod.*, *81*(2), 111–120, doi:10.1007/s00190-006-0093-1.

Grejner-Brzezinska, D. A., P. Wielgosz, I. Kashani, D. A. Smith, P. S. J. Spencer, D. S. Robertson, and G. L. Mader (2004), An analysis of the effects of different network-based ionosphere estimation models on rover positioning accuracy, *J. Global Position. Syst.*, *3*(1–2), 115–131.

Hernández-Pajares, M., J. M. Juan, J. Sanz, R. Orus, A. Garcia-Rigo, J. Feltens, A. Komjathy, S. C. Schaer, and A. Krankowski (2009), The IGS VTEC maps: A reliable source of ionospheric information since 1998, *J. Geod.*, *83*, 263–275.

Krankowski, A., and I. I. Shagimuratov (2006), Impact of TEC fluctuations in the Antarctic ionosphere on GPS positioning, *Artif. Satell.*, *41*(1), 43–56, doi:10.2478/v10018-007-0005-5.

Lukaszyk, S. (2004), A new concept of probability metric and its applications in approximation of scattered data sets, *Comput. Mech.*, *33*, 299–304, doi:10.1007/s00466-003-0532-2.

Mannucci, A. J., B. D. Wilson, D. N. Yuan, C. H. Ho, U. J. Lindqwister, and T. F. Runge (1998), A global mapping technique for GPS-derived ionospheric total electron content measurements, *Radio Sci.*, *33*(3), 565–582, doi:10.1029/97RS02707.

Park, J., V. Sreeja, M. Aquino, L. Yang, and C. Cesaroni (2015), Mitigation of ionospheric effects on GNSS positioning at low latitudes, *Proceedings of ION GNSS + 2015*, Institute of Navigation, Tampa, Florida, 14–18 September 2015.

Saastamoinen, J. (1972), Contributions to the theory of atmospheric refraction, *Bull. Geod.*, *105*(1), 279–298.

Schaer S., W. Gurtner, and J. Feltens (1998), IONEX: The IONospehre map eXchange format version 1, *Proceedings of the IGS AC Workshop*, Darmstadt, Germany, 9–11 Feb.

Shepard D. (1967), A two-dimensional interpolation function for irregularly spaced data, Proceedings of the 23rd National Conference ACM.

Spogli, L., L. Alfonsi, V. Romano, G. De Franceschi, J. F. G. Monico, M. Hirokazu Shimabukuro, and M. Aquino (2013), Assessing the GNSS scintillation climate over Brazil under increasing solar activity, *J. Atmos. Sol. Terr. Phys.*, *105*, 199–206.

Sreeja V., M. Aquino, and Z. G. Elmas (2011), Impact of ionospheric scintillation on GNSS receiver tracking performance over Latin America: Introducing the concept of tracking jitter variance maps, *Space Weather*, *9*, S10002, doi:10.1029/2011SW000707.

Sreeja V., M. Aquino, Z. G. Elmas, and B. Forte (2012), Correlation analysis between ionospheric scintillation levels and receiver tracking performance, *Space Weather*, *10*, S06005, doi:10.1029/2012SW000769.

Teunissen P. J. G. (1994), A new method for fast carrier phase ambiguity estimation, *Proceedings IEEE PLANS*, pp. 562–573, Las Vegas, Nev., 11–15 April.

Van Dierendonck A. J., Q. Hua, and J. Klobuchar (1993), Ionospheric scintillation monitoring using commercial single frequency C/A code receivers, *6th International Technical Meeting of the Satellite Division of the Institute of Navigation GPS 93*, Salt Lake City, Utah, 22–24 Sept.

Wang, J., M. Stewart, and M. Tsakiri (1998), A discrimination test procedure for ambiguity resolution on-the-fly, *J. Geod.*, *72*, 644–653.